Critical behavior of the three-dimensional random-anisotropy Heisenberg model

J. J. Ruiz-Lorenzo

*Departamento de Física and Instituto de Computación Científica Avanzada (ICCAEx), Universidad de Extremadura, 06071 Badajoz, Spain
and Instituto de Biocomputación y Física de Sistemas Complejos (BIFI), 50018 Zaragoza, Spain*

M. Dudka

*Institute for Condensed Matter Physics, National Academy of Sciences of Ukraine, UA-79011 Lviv, Ukraine
and $\mathbb{L}^4$ Collaboration and Doctoral College for the Statistical Physics of Complex Systems, Leipzig-Lorraine-Lviv-Coventry,
D-04009 Leipzig, Germany*

Yu. Holovatch

*Institute for Condensed Matter Physics, National Academy of Sciences of Ukraine, UA-79011 Lviv, Ukraine;
$\mathbb{L}^4$ Collaboration and Doctoral College for the Statistical Physics of Complex Systems,
Leipzig-Lorraine-Lviv-Coventry, D-04009 Leipzig, Germany;
Centre for Fluid and Complex Systems, Coventry University, Coventry, CV1 5FB, United Kingdom;
and Complexity Science Hub Vienna, 1080 Vienna, Austria*

We have studied the critical properties of the three-dimensional random anisotropy Heisenberg model by means of numerical simulations using the Parallel Tempering method. We have simulated the model with two different disorder distributions, cubic and isotropic ones, with two different anisotropy strengths for each disorder class. For the case of the anisotropic disorder, we have found evidence of universality by finding critical exponents and universal dimensionless ratios independent of the strength of the disorder. In the case of isotropic disorder distribution the situation is very involved: we have found two phase transitions in the magnetization channel which are merging for larger lattices remaining a zero magnetization low-temperature phase. Studying this region using a spin-glass order parameter we have found evidence for a spin-glass phase transition. We have estimated effective critical exponents for the spin-glass phase transition for the different values of the strength of the isotropic disorder, discussing the crossover regime.

I. INTRODUCTION

Structurally disordered systems apart from fundamental interests are also important for modern technology. For instance, recently developed rare-earth based magnetic glasses with magnetocaloric effects were considered as good candidates for magnetic refrigerants (see, e.g., [1]). These rare-earth based systems belong to a wide class of disordered materials [2,3] known as random-anisotropy magnets.

Magnetic properties of these systems are described by random anisotropy model (RAM), in which each spin is subjected to a local anisotropy of random orientation with the Hamiltonian [4]:

$$\mathcal{H} = -J \sum_{\langle \boldsymbol{r}, \boldsymbol{r}' \rangle} \boldsymbol{S}_{\boldsymbol{r}} \cdot \boldsymbol{S}_{\boldsymbol{r}'} - D \sum_{\boldsymbol{r}} (\hat{\boldsymbol{x}}_{\boldsymbol{r}} \cdot \boldsymbol{S}_{\boldsymbol{r}})^2. \qquad (1)$$

Here $\boldsymbol{S}_{\boldsymbol{r}}$ is a classical m-component unit vector on the site $\boldsymbol{r}$ of a d-dimensional (hyper)cubic lattice, $D > 0$ is the strength of the anisotropy, and $\hat{\boldsymbol{x}}_{\boldsymbol{r}}$ is a (quenched) random unit vector pointing in the direction of the local anisotropy axis. The interaction $J > 0$ is assumed to be ferromagnetic. We consider the case of short-range interactions, with $\langle \cdot, \cdot \rangle$ meaning summation over pairs of nearest neighbors. The strength of the disorder is controlled by the ratio D/J. For the ordered

crystalline material, the anisotropy has a well-defined direction along one of the coordinate axes, which in turn may favor certain types of spin in-plane alignments. Obviously, the random orientations are present in the model [see Eq. (1)] only for $m > 1$. In the case $m = 1$ the random anisotropy term becomes constant and leads only to a shift of the Ising system free energy.

Experimental data from random anisotropy systems are accessible from reviews; see, e.g., Refs. [5,6]. The RAM was also an object of extensive theoretical and numerical studies reviewed in Refs. [7,8]. Despite the efforts made so far, the problem of the nature of a low-temperature phase in random anisotropy magnets remains a most controversial issue. In particular, the question of whether the low-temperature phase is long-range ferromagnetically ordered or is it a spin glass. Local anisotropy prevents fully ferromagnetic state, where all spins align in the same direction. Therefore the term "asperomagnetic" was proposed for a magnetically ordered low-temperature state with nonzero magnetization, while the term "speromagnetic" was coined for the spin-glass-like state with zero magnetization [9]. Within phenomenological theory the last state is also called "correlated spin glass" [10]. Another possible candidate for the low-temperature phase in RAM is a quasi-long-range

034123-1

order (QLRO), i.e., the low-temperature ordering typical for the Berezinskii-Kosterlitz-Thouless transition [11,12], where the pair correlation function is characterized by a power-law decay with distance while the magnetization is zero.

Influence of the local anisotropy axis distributions on the critical behavior of RAM is of particular interest. The studies performed so far agree on the fact that the form of the distribution is crucial for the critical behavior of RAM. In the next section we will review results of previous studies. We will concentrate mainly on the two mentioned issues: origin of the low-temperature phase and the role of the local anisotropy axis distribution. We will leave out of scope several other challenging topics, such as dynamical aspects of phase transitions in RAM [13], effects of long-range correlations of local anisotropy axes [14], or the presence of a surface [15].

We will do this with a purpose to emphasize the main goal of our paper: In the current situation it is of primary importance to apply the state-of-the-art numerical techniques to get a high accuracy quantitative description of the critical behavior of three-dimensional Heisenberg model with moderate quenched random anisotropy in order to confront predictions of the most recent analytic calculations based on perturbative renormalization group (RG).

To this end, we will use the Parallel Tempering (PT) method and carefully study low-temperature behavior of three-dimensional RAM at $m = 3$ for two different local anisotropy axis distributions, the discrete and the continuous one, taking different values of the anisotropy strength for each distribution.

The outline of the rest of the paper is as follows. We review theoretical and numerical studies of RAM focusing mainly on results for the three-dimensional case in Sec. II. Next, we will describe our numerical simulations (simulating two different distributions of anisotropy axis) in Sec. III. Our results are displayed in Sec. IV, and finally we will discuss them and state the conclusions in Sec. V. Technical details of numerical simulations and a description of the analysis methods and the numerical study of the three-dimensional $O(3)$ model, the two-dimensional $O(2)$ model (as a proxy of a model with QLRO), and the three-dimensional Edwards-Anderson model (a classic spin glass) are given in seven Appendixes.

II. REVIEW

A. Theoretical results

First, we will describe the theoretical results regarding the isotropic disorder distribution.

The earliest theoretical investigations of the RAM were performed within the mean-field framework. Ferromagnetism was predicted [4,16], but the possibility of a spin-glass (SG) phase [17] was not excluded. An exact solution of the infinite-range interaction limit of the RAM within the mean-field approach indicates a second-order phase transition to ferromagnetic (FM) phase [18]. Such a transition was also corroborated by $1/d$ expansions [19], as well as within mean field and RG for the $m = 2$ case [20]. However, local mean-field theory [21] predicts the breakdown of long-range FM order.

Following the arguments of Imry and Ma [22] formulated for the random-field model it was shown that the $d = 3$ ran-

dom anisotropy magnet should break into magnetic domains of size $L \sim (J/D)^2$ [23] for weak anisotropy, and thus no ferromagnetism was expected. We will discuss this point in more detail in Sec. II C.

An account of fluctuations within the field theoretical RG approach [24] leads to an absence of phase transition. In the pioneer RG calculations performed for RAM with *isotropic distribution* of $\hat{x}_r$ [25] no stable accessible fixed point of the RG transformation was found in the first order of the $\varepsilon = 4 - d$ expansion. Moreover, the effective Hamiltonian for such a distribution at large D was shown to reduce to one that is similar to the effective Hamiltonian of the random-bond Ising spin glass [26], demonstrating a possibility of a SG phase in this case.

Several arguments were used in order to demonstrate an absence of the FM order for space dimensions $d < 4$ in RAM [27]. Although among these arguments the one for the limit $m \to \infty$ [27] appeared to be erroneous [28], the lack of ferromagnetism for the RAM with *isotropic distribution* of anisotropy axes for $d < 4$ was further supported by a Mermin-Wagner-type proof [29] using the replica trick [30] for the $m = 2$ case. The perturbative Migdal-Kadanoff RG studies [27,28] also suggested dimensional reduction for RAM: critical behavior of this random system at $d > 4$ is the same as for the corresponding pure system with dimension $d - 2$.

The one-loop result [25] for the absence of the second-order phase transition into a ferromagnetic state was corroborated by two- [3,8,31,32] and five-loop [33] calculations within the field-theoretical RG refined by resummation techniques.

The infinitely strong anisotropy limit of the RAM (which makes spins to be frozen in directions of local anisotropy axes and the Hamiltonian to be similar to that of the Ising random-bond spin-glass model) was investigated with the help of high-temperature expansions. Results of a Padé analysis [34] indicated typical spin-glass behavior for space dimension $d = 3$, while in Ref. [35] after obtaining non-power-law divergence of the susceptibility of three-dimensional RAM for $m = 2$ and no divergence in the case $m = 3$, it was concluded that the lower critical dimension for the RAM with $m = 2$ is $d_L = 3$.

The series analysis of Ref. [36] of the RAM in the infinitely strong anisotropy limit on Cayley trees predicted FM order, occurring for the number of nearest neighbors $\tilde{z} > m$ and a SG order for $\tilde{z} < m$. Results obtained in the same study [36] by Migdal-Kadanoff position space RG corroborate this outcome: $d = 3$ FM order for small m, while for large m the SG phase is obtained in the same universality class as that of the Ising spin glass with randomly distributed couplings.

Investigations of the RAM in the spherical model limit $m \to \infty$ were concentrated on the question about the possibility of a SG phase. This limit was studied by $1/m$ expansions [37–40] first. Within the replica method, a SG phase was found below $d = 4$ for arbitrary D [37,41]. Later the spin-glass solution was shown to be unstable [38]. A stable non-replica-symmetric solution was obtained for SG phase for $d < 4$ [39]. However, the study of dynamics of a SG order parameter avoiding the replica method for the RAM shows an instability of the SG phase [40]. These results found their confirmation in the mean-field treatment of the

$m \to \infty$ limit [42], where the SG phase appeared only as a feature of this limit and no SG phase was obtained for finite m. In the spherical limit a FM order was obtained for $d > 2$ and for D less than some critical value D_c, while for D larger than D_c a SG phase was obtained for arbitrary d ($D_c = 0$ for $d \leqslant 2$) [43].

An equation of state of the RAM showing a zero magnetization and an infinite magnetic susceptibility in the low-temperature phase for any m was obtained perturbatively [44]. Two-spin correlations in this phase possess a power-law decay. As mentioned above, such a phase appears to be QLRO. The estimate of the susceptibility of the low-temperature phase was corrected using scaling arguments [45], and it was found to be $\chi \sim (D/J)^{-4}$ at $d = 3$. A similar dependence of the susceptibility was obtained by other approaches [10,37]. The power law decay of spin correlations in the low-temperature phase was obtained in particular for a harmonic system with random fields [46], which is an approximation of a model with $m = 2$ if vortices are neglected. But the last result is in disagreement with calculations [47] for a model with random p-fold fields (for two-component fields and $p = 2$ it corresponds to the RAM with the two-component order parameter) where the SG phase was obtained.

The QLRO [48] was found for the RAM with $m = 3$ by the functional RG approach in the first order of $\varepsilon = 4 - d$ expansion. The functional RG study of higher rank anisotropies argued that dimensional reduction breaks down [49]. It was corroborated within two-loop functional RG [50,51]. These studies also showed that QLRO exists for RAM at $d_{LC}^* < d < 4$ and $m < 9, 4412$. Estimates based on expansions in ε and $m - m^*$ predict $d_{LC}^* > 3$; however, results obtained for small ε and $m - m^*$ should be extrapolated for large deviations with caution, as pointed out in Ref. [51]. Conditions for holding dimensional reduction were studied by $1/m$ expansions within the functional RG [52]. In Ref. [53] it was stated that all previous studies using $1/m$ expansions are not completely correct, since they do not take the large m limit of the easy axes into account. However, only the case of $D < 0$ was of main interest in that study. Recent research of the large-m limit reported a glassy character of the zero-temperature state [54].

The phenomenological theory [10] based on the continuous-field version of the Hamiltonian [Eq. (1)] and assuming correlations between randomly oriented anisotropy axes turned out to be a more appropriate approach for the interpretation of the field dependence of the experimentally observed magnetization in the ordered phase. In this approach the spin correlation function in different regimes of applied fields was analyzed [10]. In particular, the correlation length for small and zero fields was found to have the form $\xi \sim R_a(\frac{J}{R_a D})^2$, where R_a is the correlation range for random axes. Such a phase was called a correlated SG phase.

Once we have discussed the isotropic disorder distribution, we will discuss the *anisotropic* case.

It was first investigated in a RG study [25] with a distribution of anisotropic axes, restricting directions of the axes along the hypercube edges (*cubic distribution*). No accessible stable fixed point corresponding to a second-order phase transition point was found. Despite this, the possibility of a second-order phase transition into a FM phase with critical exponents of the diluted quenched Ising model for the RAM

with a cubic distribution was pointed out in Ref. [55], where a more general case was considered. Such peculiarities were observed for a more general model [56] including the RAM with *cubic distribution* of random axes as a particular case. Subsequently, this result was corroborated within a two-loop RG calculations with resummation [3,8,32,57] done directly for the RAM with *cubic distribution* showing that the critical behavior belongs to the universality class of the site-diluted Ising model. This result was further confirmed on the basis of a five-loop massive RG calculations [33]. While study of RAM with generic distribution [55,56], including *isotropic* and *cubic* distributions as particular cases, within the RG approach followed by resummation has predicted continuous phase transition of a new universality class [58], later it was demonstrated that this conclusion was based on erroneous calculations [59].

The RAM in the infinite anisotropy limit with mixed isotropic and cubic distributions was also investigated by mean-field theories [60–62]. It was found that the presence of a random cubic anisotropy stabilizes the FM phase [60]. Study in the limit $m \to \infty$ with finite $\alpha \equiv m/N$, where N is number of spins (so called α limit) [62], gives phase diagrams with FM and SG phases as well as with mixed phase where both FM and SG order parameters are nonzero.

Summing up, from the analysis of theoretical results one may conclude that while for an isotropic distribution the absence of FM ordering is expected, such ordering is possible for anisotropic distribution of the local anisotropy axis.

B. Numerical results

Most of the performed numerical simulations of the $d = 3$ RAM study the cases $D/J > 1$ or more often the infinitely strong anisotropy ($D/J \to \infty$) limit.

The earliest investigations report inconclusive results: both stability [63,64] as well as instability [65,66] of the FM order with respect to the SG phase have been reported. However, data of later investigations indicated the absence of ferromagnetism.

The restriction to the infinitely strong anisotropy limit led to a lack of long-range order in the ground state for $m = 3$ [67]. In this case, the critical exponents at the transition to a low-temperature phase were reported to be similar to those of the three-dimensional short-range Ising spin glass [68]. Results of Monte Carlo simulations [69] confirmed an absence of long-range order. Finally the most recent study of the infinitely strong anisotropy limit of RAM with $m = 3$ convincingly shows that the model in this case belongs to the class of short-range Ising spin glass with bond disorder [70,71].

On the other hand, results of a Monte Carlo study of the infinitely strong anisotropy limit of RAM with $m = 2$ show a low-temperature phase with extremely large susceptibility, power-law decay of the correlations, and vanishing magnetization [69], which is consistent with the theoretically predicted QLRO for arbitrary m and weak anisotropy [44]. That is confirmed by the result of Ref. [72], where a sharp phase transition into a low-temperature phase with power-law decay of the correlation function and no true magnetization were found. This case was also studied in the infinite

anisotropy limit [73] of a model with random twofold fields, where weak FM order was found with power-law correlations.

Numerical simulations of RAM with finite ratio of D/J reported the phase transition into the SG phase for the model with random twofold fields at $J = D$ [74]. Another Monte Carlo study of the RAM (1) with $m = 2$ and $J = D$ resulted in critical exponents with values similar to the XY-ferromagnetic transition, except that the heat capacity critical exponent was found to be positive [75].

Performing Monte Carlo calculations for the RAM Hamiltonian (1) with $m = 3$ and several values of D/J as well as at $D/J \to \infty$ the phase diagram in the plane $(D/J, T/J)$ was found [76]. There the regions of existence of magnetic and SG order were indicated, with the general conclusion that a random anisotropy Heisenberg model for small D/J has a QLRO low-temperature phase characterized by frozen power law spin correlations.

Results of a study of the model with random twofold fields at several values of D/J suggest that the system is ferromagnetic in a low-temperature phase at finite values of D/J [77].

Results reviewed above concern cases of continuous symmetry of the order parameter. Below we consider cases where orientations of spins as well as of the local anisotropy axes are limited only to several directions in m-dimensional space. In particular, studying RAM with $m = 2$, where the spins and anisotropic axes are oriented along the edges of a cube, the conventional XY second-order phase transition to the FM phase was found for weak random anisotropy [78], whereas a first-order transition to a domain-type FM phase was found for strong random anisotropy. For $m = 3$ both transitions were found to be of the first order [78].

The possibility of the existence of a QLRO phase was also obtained for $m = 3$ in the case of weak anisotropy but assuming $D/J = \infty$ for a part q of sites and $D/J = 0$ for the rest of $1 - q$ sites [79]. There the spins and anisotropic axes were chosen from the 12 directions. Results indicate that in addition to paramagnetic (PM) and the FM ordering a QLRO phase appears as an intermediate phase for some values of q.

The RAM with two-component spins is adopted to describe six-state clock model, where the direction of spins belongs to the Z_6 group, while the local anisotropy orientation is taken from the Z_3 group. The obtained low-temperature phase in this model has two-spin correlations decaying according to a power law, but no long-range magnetic order [80].

To summarize, the reviewed numerical studies agree, in general, with the theoretical predictions about the absence of long-range order for the $d = 3$ RAM with isotropic random axis distribution. However, they show the possibility of a FM order for the cases where orientations of local anisotropy axes are limited only to several directions.

An exception is given by the study of RAM with Heisenberg spins ($m = 3$) [81]. Studying the case $D/J=4$ for *isotropic* distribution and *cubic* distributions, surprisingly a second-order phase transition to a ferromagnetically ordered state (mistakenly identified as QLRO) was found with the same correlation length critical exponent. To check this outcome we performed similar computations for larger lattices and for two values of D/J. But before describing our model let us go back to the cornerstone of the argumentation of an absence of long-range order for $d = 3$ RAM, the Imry-Ma arguments.

C. Imry-Ma arguments

Imry and Ma introduced domain arguments in order to understand the low-temperature phase of random field magnets [22]. Later, similar arguments were directly applied to the random anisotropy case [6,23,48].

The existence of random directions in the RAM system can lead to its splitting into domains inside which spins are directed almost along one direction. If the typical size of the domains is L, than energy gain for system is $\sim DL^{d/2}$, whereas the loss of the surface energy per domain for the continuous symmetry order parameter can be estimated as $\sim JL^{d-2}$. Minimizing total energy from these two contributions with respect to L one gets $L \sim (J/D)^{2/4-d}$. That means that even for very small anisotropy strength RAM always should split into domain for $d < 4$. An earlier similar result was obtained by Larkin [82] in the context of a vortex lattice in a superconductor. Therefore one can find different names of the typical size of domains: Larkin length, Imry-Ma length, or Imry-Ma-Larkin length.

The validity of these arguments was questioned. Berzin, Morosov, and Sigov [83] pointed out that random-field arguments cannot be directly applied to the random-anisotropy case since the orientations of $\hat{x}_r$ in some direction of the order parameter space and opposite to it are equivalent in RAM. Moreover considering a continuous field variant of the RAM they have shown that the long-range order is possible when the distribution of $\hat{x}_r$ deviates from the isotropic one as well as the local anisotropy axis is present only on part of the sites [84].

Fisch [77] pointed out that with the presence of random vectors $\hat{x}_r$ the random anisotropy system is no longer translationally invariant. Therefore the consideration that the twist energy at the boundary scales in the same way as in nonrandom magnets, i.e., $\sim L^{d-2}$, is not correct.

Nevertheless, as can be seen below our results are in agreement with Imry-Ma arguments about the existence of the Larkin-Imry-Ma length and the absence of ferromagnetism for RAM with isotropic distribution.

III. THE MODEL AND SIMULATIONS

We have studied the Hamiltonian given by Eq. (1) with $m = 3$ on a three-dimensional lattice of linear size L and volume $V = L^3$ with periodic boundary conditions.

A. Random axis distributions

Two kinds of disorder have been simulated. In the first case, called hereafter "isotropic disorder," the random anisotropy vectors $\hat{x}_r$ have an uniform probability distribution on the sphere of unit radius

$$p(\hat{x}) = \frac{1}{4\pi}. \qquad (2)$$

The results obtained for such disorder will be called in the figures and tables IRAM.

In the second case, called cubic or "anisotropic disorder" and called hereafter ARAM, the vectors $\hat{x}_r$ point along the six semiaxes of the cubic lattice with the same probability $1/6$:

$$p(\hat{x}) = \frac{1}{6} \sum_{i=1}^{3} (\delta(\hat{x}, \hat{k}_i) + \delta(\hat{x}, -\hat{k}_i)), \qquad (3)$$

where $\hat{k}_i$ ($i = 1, 2, 3$) are the three unit vectors pointing to the three principal directions of a cubic lattice and $\delta(\hat{x}, \hat{k}_i)$ are Kronecker deltas. In our numerical calculations we fix $J = 1$; therefore anisotropy strength determines the ratio D/J. We measure temperature T in units of Boltzmann constant k_B and work mainly with the inverse temperature $\beta = 1/T$.

We have run Monte Carlo numerical simulations using the Metropolis (with 10 hits) and parallel tempering algorithms; see Refs. [85,86]. See Appendix A for more details on the parameters used in our runs and on the thermalization tests. In addition to generate the isotropic distribution we have used the standard rejection method [87].

B. Observables

In this section we will describe the observables we have simulated. The magnetization is computed as

$$M = \overline{\langle \sqrt{\mathcal{M}^2} \rangle}, \qquad (4)$$

with

$$\mathcal{M} = \frac{1}{V} \sum_r S_r, \qquad (5)$$

where, as usual, $\langle \cdots \rangle$ is the thermal average and $\overline{(\cdots)}$ denotes the average over the disorder.

Calculating powers of $\mathcal{M}$ we can get the associated susceptibility

$$\chi = V \overline{\langle \mathcal{M}^2 \rangle} \qquad (6)$$

and the Binder cumulant

$$U_4 = 1 - \frac{1}{3} \frac{\overline{\langle (\mathcal{M}^2)^2 \rangle}}{\overline{\langle \mathcal{M}^2 \rangle}^2}. \qquad (7)$$

With this definition the Binder cumulant will be asymptotically zero in a paramagnetic phase (Gaussian probability distribution of the magnetization with zero mean) and equal to $2/3$ in a ferromagnetic phase.

A definition of the correlation length on a finite lattice is [24,88]

$$\xi = \left(\frac{\chi/F - 1}{4 \sin^2(\pi/L)} \right)^{\frac{1}{2}}, \qquad (8)$$

where F is defined as the Fourier transform of the magnetization via

$$\mathcal{F}(k) = \frac{1}{V} \sum_r e^{ik \cdot r} S_r \qquad (9)$$

with

$$F = \frac{V}{3} \overline{\langle |\mathcal{F}(2\pi/L, 0, 0)|^2 + \text{two permutations} \rangle}. \qquad (10)$$

The interpretation of ξ as defined in Eq. (8) is the following (see for more details Sec. 2.3.1 of Ref. [24]): (1) in the paramagnetic region $\xi \to \xi_2^\infty$ for large L, where ξ_2^∞ is the second-moment correlation length computed in an infinite volume which is proportional to the exponential correlation length, (2) in the critical region $\xi \propto L$, and (3) in the ferromagnetic phase $\xi \sim L^{d/2}$ since $F = O(1)$ and $\chi \sim O(L^d)$.

Therefore ξ will converge to the true correlation length only for $T \geqslant T_c$. In the low-temperature phase it will diverge, and it is no longer the correlation length of the ferromagnetic phase. However, this fact is used in numerical studies to characterize the phase transition [24]. The cumulant $R_\xi = \xi/L$ will tend to zero (decreasing with L) in the paramagnetic region and will diverge (growing with L) in the ferromagnetic region. Thus, the curves of R_ξ for different lattice sizes will cross near the critical point.

For a finite system of size L, the Binder cumulant obeys

$$U_4(\beta, L) = f((\beta - \beta_c)L^{1/\nu}) + O(L^{-\omega}), \qquad (11)$$

where ν is the correlation length critical exponent, ω is the leading correction to scaling, and $f(\cdot)$ is a scaling function. Neglecting scaling corrections, the curves of the Binder cumulant as a function of the temperature for two different lattice sizes intersect in one point, indicating the approximate location of critical temperature β_c. The same behavior is expected for the dimensionless cumulant defined as a ratio of the correlation length to system size, $R_\xi = \xi/L$.

We have also computed the derivatives of the Binder cumulant ($\partial_\beta U_4$) and the correlation length ($\partial_\beta \xi$) by computing connected average values of different moments of the magnetization (and $\mathcal{F}$ in the case of ξ). The derivative for quantity $\mathcal{O}$ is calculated with the help of the total energy $\mathcal{E}$ defined by Eq. (1):

$$\partial_\beta \overline{\langle \mathcal{O} \rangle} = \overline{\partial_\beta \langle \mathcal{O} \rangle} = \overline{\langle \mathcal{O}\mathcal{E} - \langle \mathcal{O} \rangle \langle \mathcal{E} \rangle \rangle}. \qquad (12)$$

We have also corrected the bias of having a relatively small number of measures per sample: to do that we have applied a third-order extrapolation as described in Ref. [89].

To measure the lack of self-averaging we have computed the g_2 cumulant, defined as

$$g_2 = \frac{\overline{\langle \mathcal{M}^2 \rangle^2} - \overline{\langle \mathcal{M}^2 \rangle}^2}{\overline{\langle \mathcal{M}^2 \rangle}^2}. \qquad (13)$$

If g_2 goes to zero when system size L increases then susceptibility is a self-averaging quantity. Otherwise the susceptibility does not self-average (for details, see, e.g., Ref. [90]).

To analyze the spin-glass behavior in the isotropic disorder we have computed the overlap (see, e.g., Ref. [91])

$$q_r^{\alpha\beta} = S_r^{(1),\alpha} S_r^{(2),\beta}, \qquad (14)$$

where $S_r^{(1),\alpha}$ and $S_r^{(2),\beta}$ ($\alpha, \beta = 1, 2, 3$) are the components of two spin replicas $S_r^{(1)}$ and $S_r^{(2)}$ which evolve with the same disorder.[1]

---

[1] We have checked that the overlap computed as the scalar product of the spins belonging to different replicas shows the same properties as the one defined in the text.

TABLE I. Quotient method results for $D = 3$ and $D = 4$ and anisotropic disorder distribution (ARAM) from the crossing points of R_ξ for lattice sizes L_1 and L_2.

D	L_1/L_2	β_{cross}	R_ξ	ν_ξ	ν_{U_4}	η	Q_{U_4}	Q_{g_2}
3	6/12	0.6992(2)	0.5485(6)	0.756(1)	0.747(2)	0.019(3)	0 9975(2)	1.31(4)
3	8/16	0.6993(2)	0.5486(9)	0.757(5)	0.77(1)	0.026(5)	0.9978(3)	1.44(5)
3	12/24	0.69940(8)	0.550(1)	0.740(4)	0.762(7)	0.031(5)	0.9975(3)	1.30(5)
3	16/32	0.69941(7)	0.549(1)	0.726(6)	0.75(1)	0.030(6)	0.9980(4)	1.00(5)
3	24/48	0.69932(7)	0.548(2)	0.737(8)	0.76(2)	0.03(1)	0.9983(6)	1.12(6)
4	6/12	0.7073(2)	0.5383(7)	0.740(2)	0.749(4)	0.027(4)	0.9954(2)	1.17(3)
4	8/16	0.7079(2)	0.540(1)	0.751(7)	0.78(1)	0.035(6)	0.9952(4)	1.38(5)
4	12/24	0.7083(1)	0.545(1)	0.734(5)	0.76(1)	0.033(7)	0.9962(5)	1.17(5)
4	16/32	0.7082(1)	0.542(2)	0.710(8)	0.71(2)	0.036(9)	0.9943(7)	1.20(6)
4	24/48	0.70830(7)	0.545(2)	0.733(9)	0.76(2)	0.04(1)	0.9947(9)	1.26(7)

The Fourier transform of the tensor overlap reads

$$\mathcal{F}_q^{\alpha\beta}(\mathbf{k}) = \frac{1}{V} \sum_{\mathbf{r}} e^{i\mathbf{k}\cdot\mathbf{r}} q_{\mathbf{r}}^{\alpha\beta}. \tag{15}$$

In turn, the spin-glass susceptibility is

$$\chi_q = V \sum_{\alpha\beta} \overline{\langle |\mathcal{F}_q^{\alpha,\beta}(\mathbf{0})|^2 \rangle}, \tag{16}$$

and the correlation length in the spin-glass channel is

$$\xi_q = \left(\frac{\chi_q/F_q - 1}{4\sin^2(\pi/L)} \right)^{\frac{1}{2}}, \tag{17}$$

where

$$F_q = \frac{V}{3} \sum_{\alpha,\beta} \overline{\langle |\mathcal{F}_q^{\alpha\beta}(2\pi/L, 0, 0)|^2 + \text{two permutations} \rangle}. \tag{18}$$

As for the magnetization, we can define the following dimensionless observable in the spin-glass channel: $R_{\xi_q} = \xi_q/L$.

The behavior of R_{ξ_q} is analogous to that of R_ξ (see above in the text): it will go to zero in the paramagnetic phase, and it will diverge in the spin-glass one as L increases. The crossing of the different lattice size curves will mark the critical point.
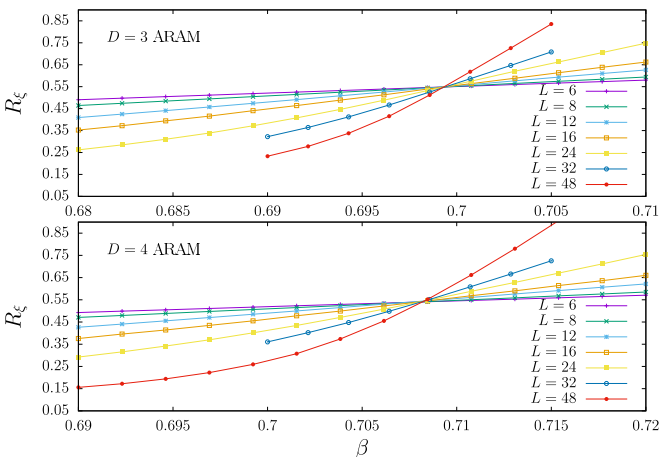

FIG. 1. R_ξ cumulant vs inverse temperature, β, for the cubic disorder for several lattice sizes.

IV. RESULTS AND ANALYSIS

We have computed the crossing points of the $R_\xi(\beta, L)$ or Binder curves of L and $2L$ lattices: $R_\xi(\beta_{\text{cross}}(L, 2L), L) = R_\xi(\beta_{\text{cross}}(L, 2L), 2L)$ or $U_4(\beta_{\text{cross}}(L, 2L), L) = U_4(\beta_{\text{cross}}(L, 2L), 2L)$. We have used a fifth-order polynomial-based analysis to compute the crossing temperatures.

Once we have found the phase transitions in the four models, we have analyzed quantitatively the behavior of the different observables using the quotient and the fixed coupling methods (see Appendix B for a description of these methods).

Furthermore, we have computed the value of R_ξ (or R_{ξ_q} in the case of a spin-glass phase transition) at β_{cross} and the value of ν_ξ from the behavior of $\partial_\beta\xi$ (the behavior of $\partial_\beta U_4$ will provide an additional estimate of the ν exponent denoted as ν_{U_4}). Finally, we have also computed η from the behavior of the susceptibility (χ) and the ratios Q_{U_4} and Q_{g_2}.

In the next two subsections we will discuss in detail our findings for the two disorder distributions.

A. Analysis of the cubic disorder

In Fig. 1 we show the behavior of R_ξ as a function of the inverse temperature β for the anisotropic disorder and $D = 3$ and 4. We also show the behavior of the Binder cumulant in Fig. 2: the signature of a phase transition is really strong for both observables, Binder cumulant and correlation length. This is manifested by the crossing of the curves for different lattice sizes near the critical point.

In addition, we have also plotted in Fig. 3 the g_2 cumulant. This cumulant shows clear crossing points (but much noisier than R_ξ and U_4), which do not extrapolate to zero (see below). This is a strong signature that the model with cubic disorder does not belong to the same universality class as a pure (nondisordered) model ($g_2 = 0$).

We start describing our findings obtained using the quotient method.

The Binder cumulant analysis presents strong scaling corrections; therefore, we will present the results of the critical parameters obtained with the analysis of the crossing temperatures of R_ξ.

The data presented in Table I show almost negligible (in our numerical precision) corrections to scaling. Hence, we
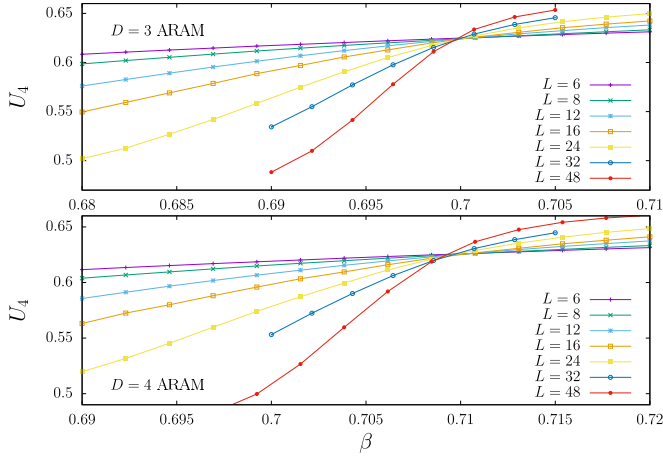
FIG. 2. Binder cumulant vs inverse temperature for the cubic disorder for several lattice sizes.

take the results for the largest pair (24 and 48) as our final estimate using the quotient method. We present the critical temperature, R_ξ cumulant at the critical point, and correlation length and pair correlation function critical exponents, ν and η, for $D = 3$ and $D = 4$ in Table II. The nonmonotonic behavior of the cumulants Q_{g_2} and Q_{U_4} (see Table I), for both values of D, precludes us from computing the ω exponent.

We have also analyzed our numerical data using the fixed coupling method. We present our estimates in Table III. In this analysis we have used only the leading term: as in the quotient method we have been unable to characterize corrections to scaling (see Appendix B). We would like to stress that the quotient and fixed coupling extrapolations are fully statistical compatible for each value of D. In addition, as a check of universality, it is important to state the statistical compatibility of all the four sets of extrapolated values (two different methods and two different values of D). The behavior of Q_{g_2} as a function of the lattice size (see Table I) is a strong hint for an asymptotic nonzero value of g_2 at the critical point, hence, ruling out that the ARAM belongs to the (pure) Heisenberg universality class for $D = 3$ and 4.
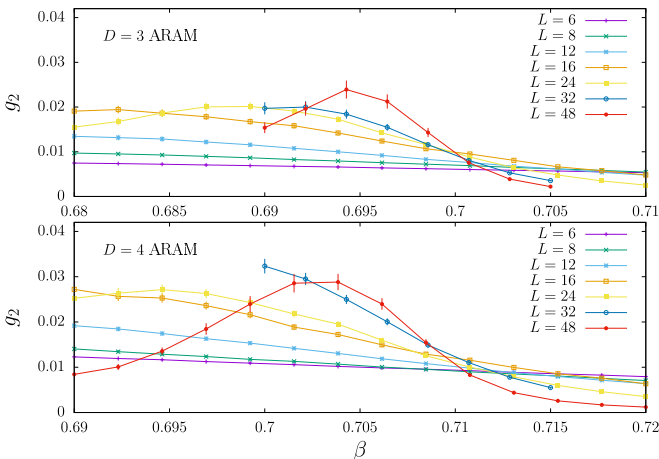

FIG. 3. g_2 cumulant as a function of the inverse temperature for the cubic disorder for several lattice sizes.

TABLE II. Inverse critical temperature, exponents, and R_ξ for the cubic disorder (ARAM), $D = 3$ and 4, obtained with the quotient method analysis of the R_ξ channel. As explained in the text, the Hamiltonian for $D = 3$ and 4 shows small corrections to scaling, and we have quoted the results obtained from the biggest lattices (24 and 48).

D	β_c	R_ξ	ν_ξ	ν_{U_4}	η
3	0.69932(7)	0.548(2)	0.737(7)	0.76(2)	0.03(1)
4	0.70830(7)	0.545(2)	0.733(9)	0.76(2)	0.04(1)

Finally we have explored the behavior of the system at very low temperatures in order to check that the system remains in the FM phase; see Fig. 4. Notice that in the FM phase R_ξ diverges with the lattice size, as is the case. Moreover, the magnetization is asymptotic (clearly nonzero), even for small lattice sizes, in the low-temperature region.

B. Analysis of the isotropic disorder

1. Magnetization channel

Let us start the study of the isotropic disorder simulating in the region, $\beta \sim 0.7$, where a phase transition was found for this disorder in the magnetic channel, for $D = 4$, in Ref. [81].

The results are shown in Fig. 5. As one can see from this figure, coming from the PM region (from higher to lower temperatures), all the R_ξ cumulant curves cross in the neighborhood of $\beta_c^1 \sim 0.7$ for all the simulated lattice sizes. This is evidence of a PM-FM continuous phase transition. A similar behavior for the Binder cumulant was also found in Ref. [81].

The crossing points of the R_ξ curves are very stable as the lattice size is growing; see Table IV. This fact allows us to determine the crossing temperatures, further denoted as $\beta_c^1(L, 2L)$, and to proceed to calculate the critical exponents using different observables. The results are described in Appendix C. However, these exponents are to be considered as "effective" ones for reasons we will explain below.

We have extended the numerical simulations, from the region $\beta \sim 0.7$ to the very low-temperature one, and, surprisingly, we have detected a clear signature of a second phase transition (marked again by the crossing points of the R_ξ curves; see Fig. 5) between a FM phase and one that we will denote as the zero magnetization phase (ZM); see below for the justification of this name. Furthermore, we denote the crossing points of this phase transition by $\beta_c^2(L, 2L)$, and we have computed them in Table IV.

A remarkable feature of the curves in Fig. 5 is that whereas the crossing points $\beta_c^1(L, 2L)$ of the first phase transition are stable with respect to changes in L, the crossing points

TABLE III. Fixed coupling method results (as described in Appendix B) for the cubic disorder (ARAM) and $D = 3$ and 4. We have used $R_\xi = 0.544$ for both values of D.

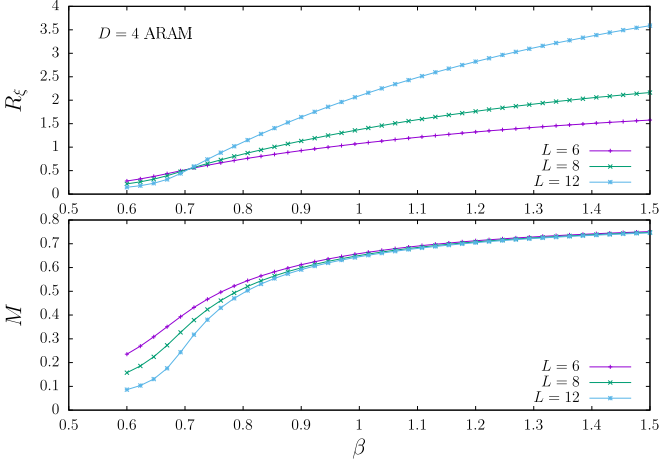| D	R_ξ	β_c	ν_ξ	ν_{U_4}	η
3	0.544	0.69941(5)	0.733(3)	0.76(5)	0.028(1)
4	0.544	0.70827(5)	0.736(3)	0.72(1)	0.035(3)

FIG. 4. R_ξ cumulant (top) and M (bottom) for $D = 4$ and cubic disorder vs the inverse temperature for the smallest simulated lattices covering a wide range of temperatures. There are no additional phase transitions in this wide range of temperatures in the magnetic channel. The magnetization M is already asymptotic for lower temperatures and small lattice sizes and is clearly nonzero.
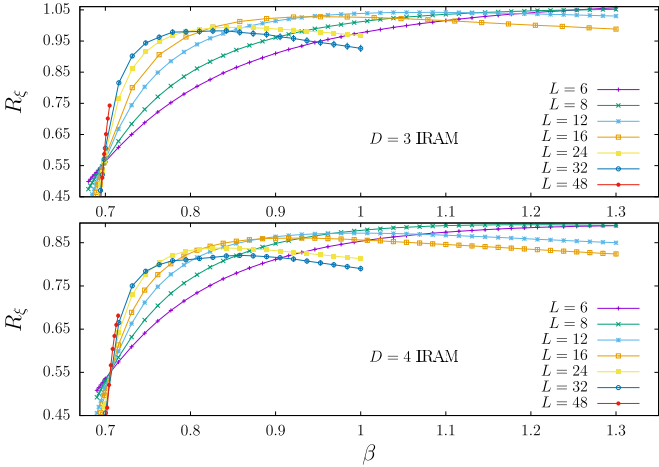

FIG. 5. R_ξ cumulant as a function of the inverse temperature for the isotropic disorder for several lattice sizes at $D = 3$ (top) and $D = 4$ (bottom).

TABLE IV. Quotient method results for $D = 3$ and $D = 4$ and isotropic disorder distribution (IRAM) from the two crossing points of R_ξ for lattice sizes L_1 and L_2.

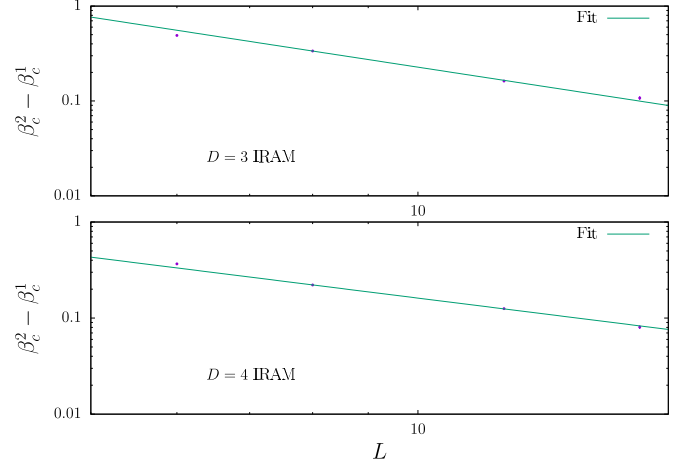| D	L_1/L_2	β_c^1	β_c^2	$\beta_c^2 - \beta_c^1$
3	6/12	0.6975(2)	1.188(1)	0.491(1)
3	8/16	0.6977(2)	1.034(2)	0.336(2)
3	12/24	0.6978(2)	0.860(3)	0.162(3)
3	16/32	0.6980(2)	0.805(5)	0.107(5)
4	6/12	0.7060(3)	1.073(1)	0.367(1)
4	8/16	0.7065(3)	0.928(2)	0.222(2)
4	12/24	0.7055(2)	0.831(2)	0.125(2)
4	16/32	0.7052(2)	0.786(4)	0.081(4)

FIG. 6. Difference of the crossing points of the first (PM-FM), $\beta_c^1(L, 2L)$, and the second (FM-ZM), $\beta_c^2(L, 2L)$, transition as a function of L for $D = 3$ (top) and $D = 4$ (bottom). The continuous lines are the fits to a pure power law, $\beta_c^2 - \beta_c^1 \propto L^{-a}$.

corresponding to the second phase transition, $\beta_c^2(L, 2L)$, show a huge drift towards the high-temperature region (i.e., towards the first phase transition). Moreover, $\beta_c^2(L, 2L)$ converges to $\beta_c^1(L, 2L)$ as the lattice size L grows, as one can see in Fig. 5.

In Table IV we report the difference between the crossing points computed as a function of the lattice size for the observed PM-FM and FM-PM transitions. For both values of D the differences scale to zero following a power law: $\beta_c^2(L, 2L) - \beta_c^1(L, 2L) \propto L^{-a}$, finding very good fits (for $L > 6$) for both values of D, with the exponent $a \simeq 1.5$ ($D = 4$) and $a \simeq 1.7$ ($D = 3$).

In Fig. 6 the difference between the crossing points of the two transitions is plotted as a function of the lattice size, where we have also plotted the pure power law.

R_ξ behaves in the low-temperature region as in the high-temperature region: R_ξ decreases as L increases (see Fig. 5) in a completely different way as in a ferromagnetic phase.

The behavior of the Binder cumulant (see Fig. 7) provides the same information. One can observe the crossing of the U_4 curves corresponding to different lattice sizes and that, for large lattice sizes and a fixed lower temperature, g_4 decreases with L, just as in a phase with a Gaussian distribution (with zero mean) of the magnetization.

In order to understand what are the properties of the low-temperature phase (we have termed ZM) we have computed the modulus of the magnetization. The behavior of the modulus of the magnetization is presented in Fig. 8 for the two values of the disorder strength. Notice that the behavior of these observables is completely different from the anisotropic case; see Fig. 4, bottom, In the latter case, one can see that the magnetization is already nonzero and independent of L for relatively small lattice sizes. However, in the isotropic case, we observe that the magnetization is not asymptotic and decreasing for $D = 3$ and 4 and for all the range of simulated temperatures.

To be more quantitative, we have analyzed the behavior of M as a function of L at $\beta = 1$ and we have obtained that $M \sim L^{-0.16}$ and $L^{-0.22}$ for $D = 3$ and 4, respectively. In addition,
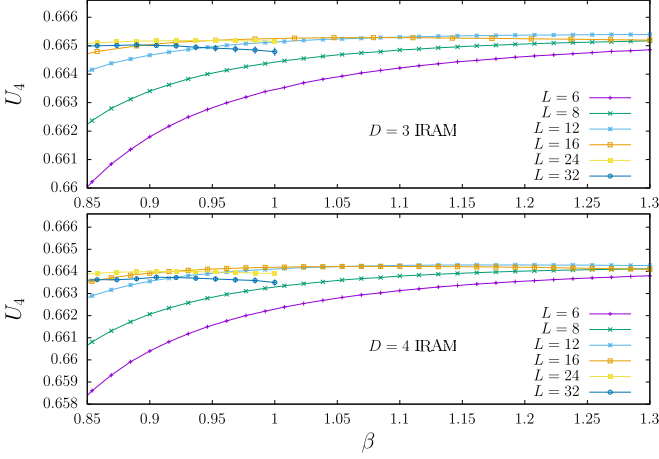
FIG. 7. Binder cumulant (U_4) as a function of the inverse temperature for the isotropic disorder for several lattice sizes at $D = 3$ (top) and $D = 4$ (bottom) in the low-temperature region. Notice the crossing of the different lattice sizes and the nonmonotonic behavior (decrease with L) for the larger lattices.

R_ξ at this $\beta = 1$ also decreases as $R_\xi \sim L^{-0.16}$ and $L^{-0.10}$ (for the larger sizes) for $D = 3$ and 4, respectively. Thus, M and R_ξ seem to go to zero as the lattice size increases.

To support this conclusion, we have explicitly checked in Appendix D that at $\beta \simeq 2\beta_c^1 \sim 1.4$ and for $D = 4$ the magnetization and R_ξ decrease with L and are well described by power laws (with the exponents similar to those obtained at $\beta = 1$), meaning that they will vanish in the thermodynamic limit. This is a strong hint that this low-temperature phase has zero magnetization and finite magnetic correlation length (ξ).

From the above observations, one can describe a strong crossover in the behavior of the isotropic disorder: for $L \gg L_c$ there is no phase transition in the magnetization channel. We are tempting to interpret this crossover length (L_c) as that proposed by Imry-Ma. Our power law fits suggest that L_c is much higher than the maximum simulated lattice size (i.e., $L = 48$) for both values of the anisotropy strength near β_c^1. Finally, in
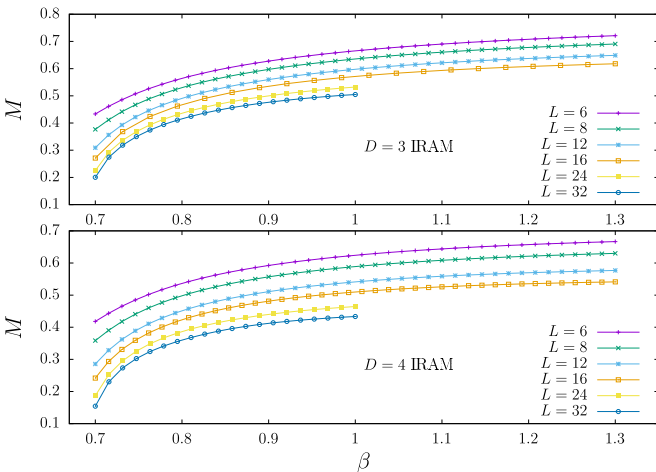

FIG. 8. Modulus of the magnetization, M, as a function of the inverse temperature for the isotropic disorder for several lattice sizes at $D = 3$ (top) and $D = 4$ (bottom).
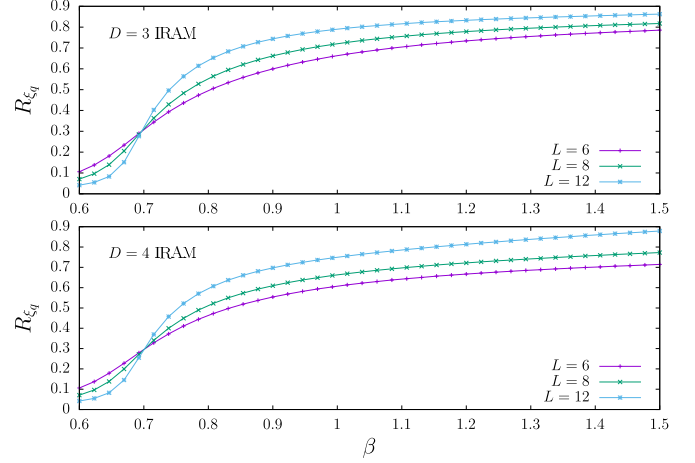

FIG. 9. R_{ξ_q} cumulant (overlap channel) as a function of the inverse temperature for the isotropic disorder for several lattice sizes for $D = 3$ (top) and $D = 4$ (bottom).

the next section we will argue in favor of the appearance of a phase with spin-glass properties as an additional argument stating the magnetization channel is not critical. We will use the word "transition" to refer to one of these two crossing regions which eventually will merge.

The main conclusion of this subsection and Appendix D is that the low-temperature phase presents zero magnetization and finite correlation length.

However, the numerical results presented in this subsection cannot completely rule out that the difference $\beta_c^1(L, 2L) - \beta_c^2(L, 2L)$ remains finite or even the magnetization is different from zero (asymptotically), although we consider this scenario unlikely since it goes against the Imry-Ma argument.

The behavior of R_ξ around the first phase "transition" (β_c^1) looks similar to that of a QLRO one due to the overall behavior of R_ξ: first it grows (due to β_c^1) and then decreases (due to β_c^2) inducing an apparent merging of the R_ξ in the interval $[\beta_c^1, \beta_c^2]$, which recalls the behavior in a QLRO phase transition. In a QLRO phase the curves of $R_\xi = \xi/L$ merge because the correlation length is divergent in the whole low-temperature phase. See Appendix E for the behavior of R_ξ and the Binder cumulant of the two-dimensional XY model which undergoes this QLRO phase transition.

2. Overlap channel

In this subsection we will characterize the properties of the ZM low-temperature phase found in the previous subsection; the first candidate will be a phase with spin-glass properties: it presents zero magnetization, and it is not critical in the magnetic channel. The presence of a low-temperature phase with spin-glass properties has been previously reported (e.g., see Refs. [76,92]).

To this end, we will analyze the behavior of R_{ξ_q} defined using the overlap correlation length; see Eq. (17). To proceed further, we have simulated two real replicas (the same disorder) of the model and computed the overlap, Eq. (14), which characterizes a spin-glass phase. Additionally, we have computed the associated R_{ξ_q}.
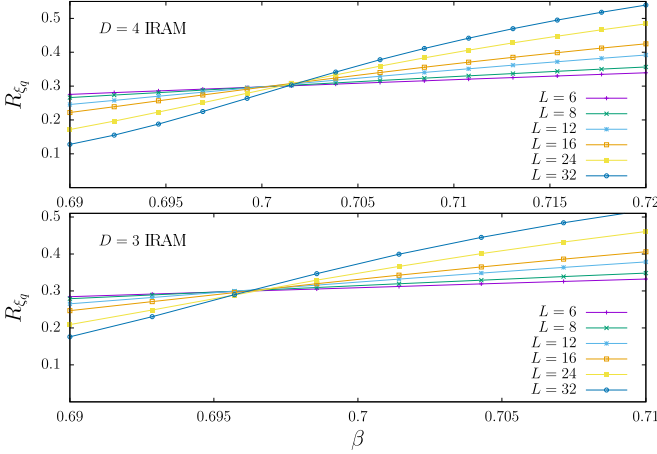
FIG. 10. Near the PM-SG phase transition: R_{ξ_q} cumulant (overlap channel) as a function of the inverse temperature for the isotropic disorder for several lattice sizes at $D = 4$ (top) and $D = 3$ (bottom).

In Fig. 9 we show the behavior of R_{ξ_q} in a wide range of inverse temperatures for the simulated lattice sizes: the curves cross in the region near $\beta \sim 0.70$.

As we have discussed in the previous subsection (see also Appendix D), the spontaneous magnetization vanishes in the very low-temperature region: in this region $R_{\xi_q} = \xi_q/L$ diverges as corresponds to the spin-glass phase. Notice that ξ_q is a true correlation length in the paramagnetic phase. In the spin-glass phase R_{ξ_q} diverges as L increases [24,93].

We would like to remark that, for instance, at $\beta = 1.3$ (and for both values of D), R_ξ decreases monotonically with L (magnetic channel) and R_{ξ_q} increases monotonically with L (overlap channel), for all the simulated values of L.

In Appendix F we show the behavior of the three-dimensional Edwards-Anderson model, a spin glass, in both the magnetic and the overlap channels. In this case, the system presents a clear crossing of the different R_{ξ_q} curves and no signal in the Binder and R_ξ in the magnetic channel (in this case both observables are just compatible with zero, showing no critical behavior).

Summing up, the results shown in Fig. 9 point to a low-temperature phase with the properties of a spin glass.[2]

Hence, the analysis in the overlap channel gives additional weight to the observations made for the magnetization channel: the PM-FM and the FM-PM "transitions" merge for large L and the final outcome is the absence of a FM phase for all positive temperatures. Notice that the vanishing of R_ξ shows that the magnetic correlation length is finite, and this phase is not critical in the magnetization channel. In particular this result ruled out the QLRO scenario.

We have also performed a detailed study of the crossing region of R_{ξ_q} for both values of D. In Fig. 10 we show the behavior of R_{ξ_q} in the crossing region. The corresponding crossing points and associated critical exponents (computed with the quotient method) are presented in Table V.

___

[2]The system could present a complicated antiferromagnetic low-temperature order inducing the reported phenomenology of the isotropic disorder [94], but, we consider this scenario very unlikely.

TABLE V. Quotient method results for $D = 3$ and $D = 4$ and isotropic disorder distribution (IRAM) from the crossing points of R_{ξ_q} (SG channel) for lattice sizes L_1 and L_2.

D	L_1/L_2	β_{cross}	R_{ξ_q}	ν_ξ	η_q
3	6/12	0.6955(3)	0.298(1)	0.776(4)	1.03(1)
3	8/16	0.6965(3)	0.302(1)	0.789(4)	1.04(1)
3	12/24	0.6969(2)	0.306(2)	0.797(5)	1.04(2)
3	16/32	0.6962(2)	0.300(2)	0.778(6)	1.06(2)
4	6/12	0.6999(2)	0.2973(8)	0.799(3)	1.02(1)
4	8/16	0.7003(2)	0.299(1)	0.804(4)	1.03(1)
4	12/24	0.7014(2)	0.305(2)	0.822(6)	1.02(2)
4	16/32	0.7020(2)	0.311(2)	0.818(7)	1.00(2)

Our results point to (see Table V) $\nu \sim 0.78$–0.82 for both values of D. In addition, we do not see the growing of the ν exponent with L as seen in the magnetization channel. In addition, the computed exponent is very different from that reported for Ising and Heisenberg spin-glass models; see Table VI.

However, we have for η a big value, near 1. The overlap q and the magnetization m have different scaling dimensions, d_q and d_m, correspondingly. Roughly $q \sim m^2$, so that $d_q \simeq 2d_m$. Substituting in this estimate $2d_m = d - 2 + \eta$ and $d_q = (d - 2 + \eta_q)/2$ one gets for $d = 3$ and $\eta(d = 3) \simeq 0$ (see Table X of Appendix C) $\eta_q = 1 + 2\eta \simeq 1$ in very good agreement with the η_q values reported in Table V. This is the consequence of simulating lattice sizes smaller than the (Imry-Ma) crossover length in the critical region. From previous discussion, the value of this crossover length at very low temperatures is small, allowing us to monitor the decreasing of the magnetization and R_ξ for the lattice sizes we have been able to simulate.

Therefore, the exponents of Table V can be considered only as effective ones. The simplest explanation is that they first attain the PM-FM values (in a ferromagnetic phase $q \propto m^2$), and eventually they will cross over to the PM-SG ones in the asymptotic limit (where the magnetization is zero with a nonvanishing overlap), since we are simulating lattice sizes below the Imry-Ma length.

V. CONCLUSIONS AND DISCUSSION

We have simulated the RAM with cubic and isotropic disorder in three dimensions. To do that, we have run very large numerical simulations using PT (and Metropolis as the local update method) simulating large lattice sizes ($L = 48$).

This model was also studied in Ref. [81] by means numerical simulations and using the PT algorithm for cubic and isotropic disorder distributions near $\beta \sim 0.7$. The authors

TABLE VI. Critical exponents for two related three-dimensional models undergoing PM-SG phase transitions.

Model	ν	η_q
Heisenberg [95]	1.5(2)	−0.19(2)
Edwards-Anderson (Ising) [96]	2.56(4)	−0.390(4)

TABLE VII. Critical exponents and cumulants for three three-dimensional related models undergoing PM-FM phase transitions.

Model	ν	η	ω	R_ξ	U_4	g_2
Heisenberg [97–99]	0.7116(10)	0.0378(3)	0.773	0.5639(2)	0.6202(1)	0
Ising (site-diluted) [93]	0.6837(53)	0.037(4)	0.37(6)	0.598(4)	0.449(6)	0.145(3)
Ising [100,101]	0.629912(86)	0.0362978(20)	0.8303(18)	0.6431(1)	0.46548(5)	0

simulated only $D = 4$ and $L \leqslant 24$. They found clear crossing of the different Binder cumulant curves for both distributions. Despite this, the authors claimed that the low-temperature phase is in the QLRO class. They computed only the ν exponent by studying the susceptibility, quoting for both disorders $\nu = 0.70998$ with 0 as a statistical error, hence, claiming that both disorders belong to the same universality class. In addition they reported $\beta_c = 0.70998(4)$ for ARAM and $\beta_c = 0.70435(2)$ for IRAM. In this work, we report estimates of β_c and ν for $D = 4$ not compatible with those of Ref. [81] for the anisotropic disorder. In addition for isotropic disorder, we have characterized how the two phase transitions eventually merge and the low-temperature phase can be consistently described by a phase with spin-glass properties.

In the previous section, we have discussed the critical behavior for both disorder distributions. Since it is clear that the critical behavior of these two distributions is different we will discuss separately our findings for each distribution.

A. Cubic disorder

We have found a phase transition between a PM phase and a FM one. Both values of the strength of the anisotropy, D, provide critical exponents and cumulants compatible in the statistical error, a fact which supports the universality of this disorder for moderate values of D.

Notice that our estimates for the critical exponents and cumulants are completely different from the Heisenberg model ones (see Table VII). Moreover, we have simulated the pure Heisenberg model within the PT method and used the same procedure of analysis as used in this paper. The obvious conclusion is that ARAM and Heisenberg models belong to different universality classes; cf. Table XIII of Appendix G.

Furthermore our results do not agree with the perturbative RG predictions [32,33,55–57,59], which state that the ARAM should belong to the same universality class as the three-dimensional site-diluted Ising model, as follows from comparison of our values for the critical exponents from Tables II and III with the Monte Carlo results of Table VII for the three-dimensional site-diluted Ising model. The latter are corroborated also by RG studies; see, e.g., Refs. [102–104].

The following scenario emerges from our simulations: the anisotropic disorder, as predicted by RG, is relevant and changes the universality class of the pure model. We have checked that this scenario holds for $D \leqslant 4$. We expect this fixed point should be relevant for $0 < D < D_c$. We can try to conjecture the behavior of the model with anisotropic disorder for strong anisotropy. For large $D > D_c$ the anisotropic disorder will destroy the FM phase and a SG phase will arise. We know that for $D = \infty$ the system is described by the Ising spin-glass universality class [70,71]. Open problems are the characterization of D_c and to figure out the universality class

for $D_c < D < \infty$: is that of the Ising spin-glass model in three dimensions?

B. Isotropic disorder

We have found two different crossing regions of the cumulant R_ξ (and of the U_4 cumulant). Furthermore, these two regions seem to merge, a clear indication of a phase with zero magnetization for all the positive temperatures. We have checked this scenario by studying the behavior of the magnetization and R_ξ at very low temperatures. This result is in full agreement with the Imry-Ma arguments that predict zero magnetization for $T > 0$. Note that Imry-Ma domain arguments were also corroborated recently by extensive Monte Carlo simulations for two-dimensional random anisotropy magnets [105].

Studying the overlap channel we have found a phase transition between a paramagnetic phase and a phase with spin-glass properties, and we have characterized its critical exponents. However, taking into account that the (Imry-Ma) crossover length around the transition is much larger than the largest simulated lattice size, we consider these exponents as effective ones.

A low-temperature phase with spin-glass properties was reported in Ref. [92] studying the isotropic disorder model simulating (out-of-equilibrium) a $L = 20$ lattice for $D = 3.5$. They found that the field-cooled and zero-field-cooled magnetization behave, in the low-temperature region, in the same way as in a spin glass [94].

TABLE VIII. Parameters used in the numerical simulations for the cubic disorder distribution (ARAM). N_{samples} is the number of disorder realizations, N_T is number of temperatures in the parallel tempering, and N_{sweeps} number of Monte Carlo sweeps per temperature.

D	L	N_{samples}	N_T	N_{sweeps}
3	6	13 600	14	10^5
3	8	4800	14	10^5
3	12	2937	14	10^5
3	16	2000	14	1.28×10^5
3	24	2091	14	1.28×10^5
3	32	1400	8	2.56×10^5
3	48	392	8	5.12×10^5
4	6	13 600	14	10^5
4	8	4800	14	10^5
4	12	2938	14	10^5
4	16	2000	14	1.28×10^5
4	24	2068	14	2.56×10^5
4	32	1400	8	2.56×10^5
4	48	768	14	5.12×10^5

TABLE IX. Parameters used in the numerical simulations for the isotropic disorder distribution (IRAM) near β_c^1.

D	L	N_{samples}	N_T	N_{sweeps}
3	6	13 600	14	10^5
3	8	4800	14	10^5
3	12	3000	14	10^5
3	16	2000	14	1.28×10^5
3	24	2075	14	1.28×10^5
3	32	1400	8	2.56×10^5
3	48	400	8	5.12×10^5
4	6	17 600	14	10^5
4	8	4800	14	10^5
4	12	3000	14	10^5
4	16	2000	14	1.28×10^5
4	24	2000	14	2.56×10^5
4	32	1400	8	2.56×10^5
4	48	400	8	1.024×10^6

FIG. 11. Effective critical behavior in vicinity of β_c^1: R_ξ cumulant as a function of the inverse temperature for the isotropic disorder for several lattice sizes.

Our work provides additional arguments (from equilibrium numerical simulations) supporting a low-temperature phase for the isotropic disorder with spin-glass behavior and zero magnetization.

An important open problem is to try to compute the asymptotic exponents of this PM-SG transition and to study how the model leads to the Ising Edwards-Anderson universality class for $D = \infty$ [70,71]. We consider that such study is outside of the currently available computational resources.

ACKNOWLEDGMENTS

APPENDIX A: NUMERICAL SIMULATION DETAILS

We have performed extensive Monte Carlo numerical simulations using the Metropolis (with 10 hits) and PT algorithms; see Refs. [85,86]. We have checked that the PT is correctly working with our choice of the different parameters.

In order to have an additional test of the thermalization of our systems, we have studied the behavior of different observables at all the temperatures as a function of $\log t$ (t being the Monte Carlo time). We consider that we have thermalized the system, for a given observable, when the last three points are compatible in the error bars and a plateau can be defined (the last point is computed with the last half of the Monte
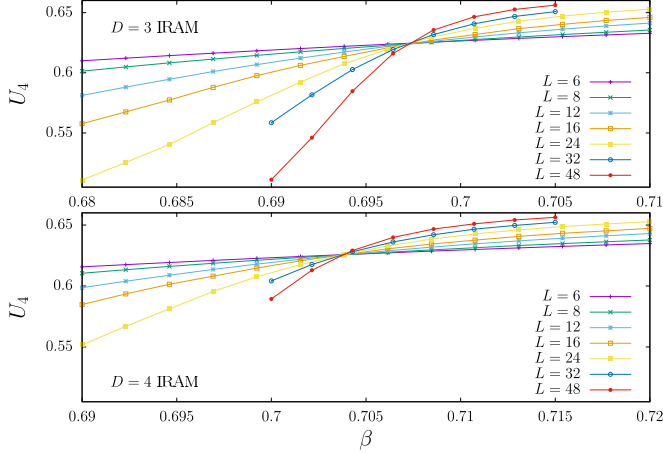
TABLE X. Quotient method results for $D = 3$ and $D = 4$ and isotropic disorder distribution (IRAM) from the crossing points of R_ξ for lattice sizes L_1 and L_2 near β_c^1.

D	L_1/L_2	β_{cross}	R_ξ	ν_ξ	ν_{U_4}	η	Q_{U_4}	Q_{g_2}
3	6/12	0.6975(2)	0.5540(8)	0.807(2)	0.768(2)	0.012(4)	0.9995(1)	1.64(4)
3	8/16	0.6977(2)	0.554(1)	0.828(6)	0.81(1)	0.015(5)	1.0008(2)	1.69(5)
3	12/24	0.6978(2)	0.556(2)	0.846(6)	0.83(1)	0.013(6)	1.0030(2)	1.40(5)
3	16/32	0.6980(2)	0.557(2)	0.87(1)	0.89(1)	0.00(1)	1.0049(4)	1.18(4)
3	24/48	0.6975(2)	0.552(3)	0.92(2)	0.90(2)	0.01(2)	1.0033(6)	1.4(1)
4	6/12	0.7060(3)	0.551(1)	0.896(4)	0.869(4)	−0.004(5)	1.0024(2)	1.36(2)
4	8/16	0.7065(3)	0.553(2)	0.98(1)	0.97(2)	−0.012(7)	1.0049(3)	1.31(4)
4	12/24	0.7055(2)	0.548(2)	0.98(1)	1.01(2)	−0.007(9)	1.0048(4)	1.28(4)
4	16/32	0.7052(2)	0.542(3)	0.97(2)	0.98(2)	−0.00(1)	1.0049(5)	1.14(4)
4	24/48	0.7055(3)	0.549(5)	1.13(5)	1.17(5)	−0.04(2)	1.0077(8)	1.04(7)

FIG. 12. Effective critical behavior in vicinity of β_c^1: Binder cumulant as a function of the inverse temperature for the isotropic disorder for several lattice sizes.

FIG. 14. R_ξ and U_4 cumulants vs inverse temperature for the two-dimensional $O(2)$ pure model on different lattice sizes. We have also plotted $\beta_c = 1.1199(1)$, $R_\xi = 0.7506912$, and $U_4 = 0.660603(12)$.

Carlo history). All the results presented in this study fulfill this thermalization criteria.

We will provide the parameters of the different numerical simulations for the models with $D = 3$ and 4 and both types of disorder, cubic and isotropic:

Anisotropic Disorder:

(1) Near the critical point. See Table VIII.

(2) Extended run. We have simulated $L = 6$, 8, and 12 for $D = 4$ using the PT method: 1000 samples, 40 temperatures, and 204 800 Monte Carlo steps for each temperature.

Isotropic Disorder:

(1) Near the critical point (Magnetization, first phase transition). See Table IX.

(2) Extended runs (Magnetization). For $D = 3$, 1000 samples and 40 temperatures (PT) have been simulated for $L = 6$, 8, 12, and 16; 400 samples and 40 temperatures (PT) for $L = 24$ and 230 samples and 20 temperatures (PT) for $L = 32$. We have performed 409 600 sweeps per temperature in the PT.
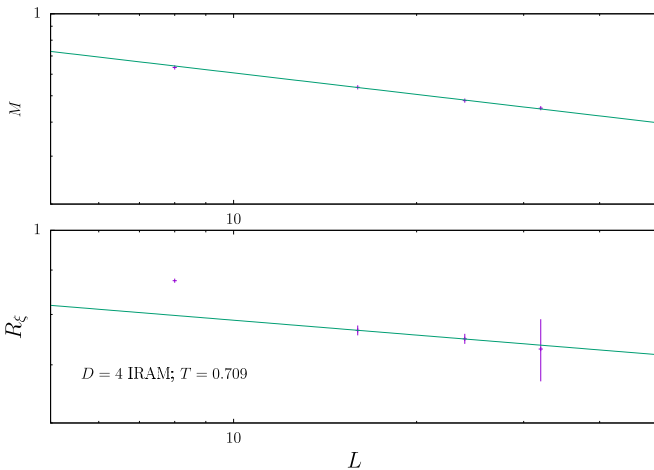
For $D = 4$, 40 temperatures (PT) have been simulated with 2000, 1200, 2000, 658, and 786 samples for $L = 6$, 8, 12, 16, and 24, respectively; 500 samples and 20 temperatures (PT) for $L = 32$. We have performed 409 600 sweeps per temperature in the PT.

(3) Extended runs (Overlap). 40 temperatures (PT) have been simulated for $L = 6$, 8, 12. For $D = 3$, we have run 1000 samples and for $D = 4$, 500 samples. We have performed 204 800/409 600 sweeps per temperature in the PT for $D = 3$ and 4, respectively.

(4) Near the critical point (overlap). For $D = 3$, we have simulated eight temperatures (PT) for $L = 6$, 8, 12, 16, 24 and 32 with 1000, 1000, 1000, 760, 500, and 500 samples respectively. For $D = 4$, we have simulated 14 temperatures (PT) for $L = 6$, 8, 12, 16, 24 and 32 with 3000, 3000, 1792, 1000, 500 and 495 samples respectively. In all cases we have performed 204 800 sweeps per temperature in the PT.

APPENDIX B: QUOTIENT AND FIXED COUPLING METHODS

In this Appendix we briefly describe the quotient and fixed coupling methods.

First, we describe the quotient method. Let $O(\beta, L)$ be a dimensionful quantity scaling in the thermodynamic limit as $\xi^{x_O/\nu}$. For a dimensionless observable the exponent $x_O = 0$. Thereafter, we will use the symbol g to denote all the dimensionless quantities, such as U_4, g_2, or R_ξ.

FIG. 13. Behavior of the magnetization per spin (top) and R_ξ (bottom) for $D = 4$ and isotropic disorder as a function of the lattice size at $T = 0.709$. The data are well described by power laws (continuous lines in both panels).
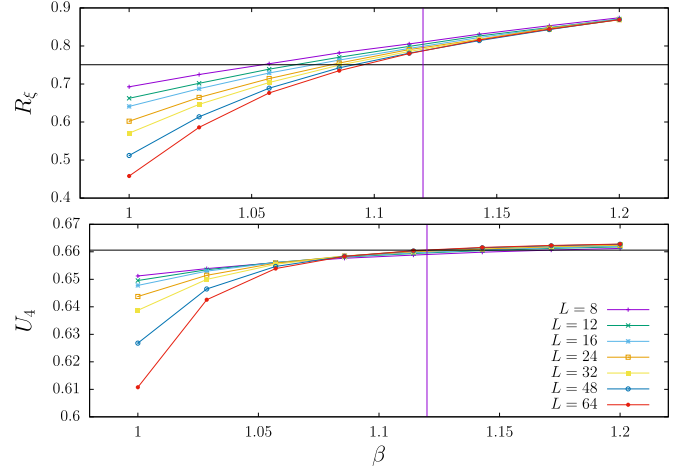
TABLE XI. Independent extrapolations of the fixed coupling method data, using the Binder cumulant $U_4 = 0.6606$, for the two-dimensional XY model.

U_4	ν_ξ	ν_{U_4}	η
0.6606	3.8(2)	3.6(3)	0.246(3)

TABLE XII. Independent extrapolations of the fixed coupling method data, using $R_\xi = 0.75$, for the two-dimensional XY model.

R_ξ	ν_ξ	ν_{U_4}	η
0.75	4.0(1)	7.0(6)	0.236(1)

The behavior of the observable O can be studied by computing, at L and $2L$, the quotient

$$\mathcal{Q}_O = \frac{O(\beta_{\mathrm{cross}}(L, 2L), 2L)}{O(\beta_{\mathrm{cross}}(L, 2L), L)}, \tag{B1}$$

where $\beta_{\mathrm{cross}}(L, 2L)$ is defined by

$$g(L, \beta_{\mathrm{cross}}(L, 2L)) = g(2L, \beta_{\mathrm{cross}}(L, 2L)). \tag{B2}$$

From the previous discussion, one can write

$$\mathcal{Q}_O^{\mathrm{cross}} = 2^{x_O/\nu} + O(L^{-\omega}) \tag{B3}$$

and

$$g^{\mathrm{cross}} = g^* + O(L^{-\omega}), \tag{B4}$$

where x_O/ν, g^* and the correction-to-scaling exponent ω are universal quantities. In order to compute the ν and η exponents, one should study dimensionful observables such as the susceptibility $[x_\chi = \nu(2 - \eta)]$ and the β derivatives of R_ξ and U_4 ($x = 1$ in both cases).

The crossing point of the inverse temperature ($\beta_{\mathrm{cross}}(L, 2L)$) behaves following the equation

$$\beta_{\mathrm{cross}}(L, 2L) = \beta_{\mathrm{c}} + A_{\beta_{\mathrm{c}}, g} L^{-\omega - 1/\nu} + \cdots. \tag{B5}$$

The leading correction-to-scaling exponent can be computed via the quotient of a given dimensionless quantity g (Q_g). The behavior of this quotient is

$$\mathcal{Q}_g^{\mathrm{cross}}(L) = 1 + A_g L^{-\omega} + B_g L^{-2\omega} + \cdots. \tag{B6}$$

Another way to compute critical exponents is to work at a fixed dimensionless observable. One fixes the value of the dimensionless observable $g = g_f$ near the universal one (for example, fixing a given value of R_ξ) and then computes $\beta(L)$ defined as

$$g_f = g(\beta(g_f, L), L). \tag{B7}$$

Using these values of the inverse temperature, one can monitor the scaling. At this value of the inverse temperature we can study the scaling of different observables (e.g., susceptibility,
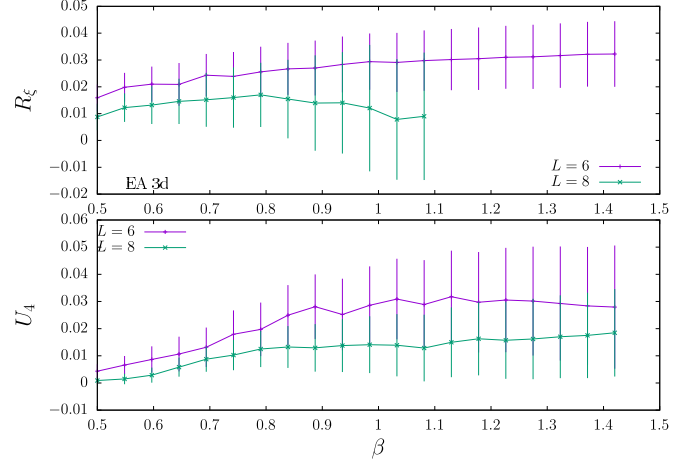

FIG. 15. Behavior of the correlation length in units of R_ξ the lattice size R_ξ (top) and the Binder cumulant U_4 (bottom) in the magnetic channel for the three-dimensional Edwards-Anderson model. For $L = 6$ and $L = 8$ both observables are almost compatible with zero. Notice that in the low-temperature region we have been unable to compute R_ξ, even simulating a huge number of samples, due a signal-noise problem (the final value is compatible with zero and the computation of R_ξ involves a square root).

derivatives of R_ξ and Binder cumulant, etc.) to extract the critical exponents using

$$O(\beta(g_f, L), L) = A(g_f) L^{x_O/\nu} \left[1 + O\left(\frac{1}{L^\omega}\right) \right]. \tag{B8}$$

APPENDIX C: THE PM-FM TRANSITION FOR THE ISOTROPIC DISORDER

We have shown numerical data based on the behavior of R_ξ with temperature and lattice sizes supporting that both phase transitions (near β_c^1 and β_c^2) are merging, eventually for lattice sizes bigger than a crossover length as stated by the Imry-Ma argument.

In this Appendix we report the values of the critical exponents of the PM-FM transition observed for IRAM at temperature $T \sim 1/\beta_c^1$. As we have shown in the main text, this phase transition should disappear for large lattice sizes. Therefore the reported below values of the exponents characterize the effective critical behavior of the model at least for $L \leqslant 48$. This behavior is observed before the PM-FM

TABLE XIII. Quotient method results for the pure $O(3)$ model ($D = 0$) from the crossing points of R_ξ for lattice sizes L_1 and L_2. The numbers in round brackets are the statistical error of the fit and the number inside the square ones are systematic errors originating from the uncertainty in the ω exponent used in the fit.

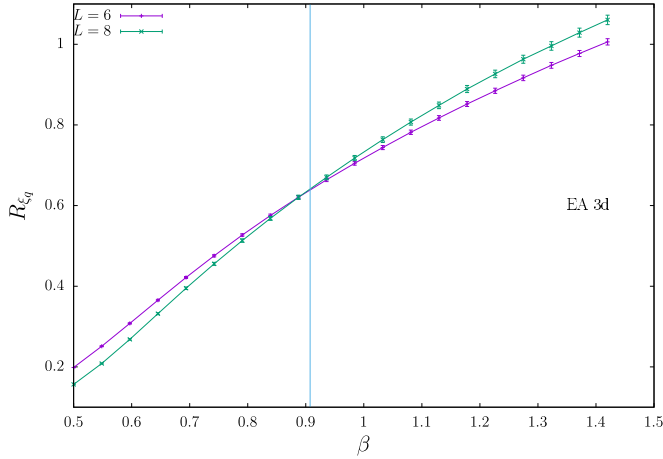| L_1/L_2	β_{cross}	R_ξ	ν_ξ	ν_{U_4}	η	Q_{U_4}
6/12	0.692577(7)	0.5567(5)	0.727(3)	0.697(7)	0.024(2)	0.9966(3)
8/16	0.69283(3)	0.5587(3)	0.718(3)	0.699(5)	0.029(2)	0.9972(2)
12/24	0.69290(2)	0.5597(5)	0.716(3)	0.705(7)	0.034(2)	0.9982(2)
16/32	0.69293(2)	0.5601(4)	0.714(4)	0.706(7)	0.037(2)	0.9986(2)
24/48	0.69298(1)	0.5617(4)	0.717(6)	0.72(1)	0.036(3)	0.9990(3)
∞	0.6930(3)	0.5630(5)[6]	0.708(4)[2]	0.717(9)[2]	0.043(2)[2]	$\omega = 0.92(13)$

FIG. 16. Behavior of the overlap correlation length in units of the lattice size R_{ξ_q} vs the inverse temperature for the three-dimensional Edwards-Anderson model for small lattice sizes. Notice that both curves cross, marking the apparent critical temperature of the model. The vertical line marks the infinite volume critical inverse temperature $\beta_c = 0.908(2)$ [96].

transition point β_c^1 merges with FM-PM transition point β_c^2 moving from the low-temperature region.

In Figs. 11 and 12 we show the behavior of R_ξ and U_4 in the vicinity of the first phase transition temperature β_c^1. We have analyzed the isotropic disorder in the same way as the cubic one (see Sec. IV A), focusing on the analysis of the crossing temperatures of R_ξ since the Binder cumulant data present strong corrections to scaling.

We report in Table X our results. Note that our estimates of the effective critical exponents and cumulants are different from the pure Heisenberg ones. Moreover, the ν exponent is measurably growing with the disorder strength, which is the right behavior in view of the onset of a second phase transition merging with this one.

Finally, we recall that the Imry-Ma characteristic lengths for these values of D is much bigger than $L = 48$.

APPENDIX D: THE MAGNETIZATION AND R_ξ AT VERY LOW TEMPERATURE FOR ISOTROPIC DISORDER WITH STRENGTH $D = 4$

In this Appendix we analyze the behavior of the magnetization at very low temperature.

To compute the magnetization at $T \simeq T_c^1/2 = 1/(2\beta_c^1) \simeq 0.709$ we have resorted to the use of a out-equilibrium dynamical approach consisting in the computation of the magnetization and R_ξ as a function of time, starting from ordered and fully disordered configurations, and to extrapolate both simulations to the same asymptotic value using power laws: $m_\infty + O(t^{-x_m})$ or $R_\xi = R_{\xi_\infty} + O(t^{-x_{R_\xi}})$.

We have simulated $L = 8$ (400 samples and 2 048 000 Monte Carlo steps), $L = 16$ (300 samples and 2 048 000 Monte Carlo steps), $L = 24$ (200 samples and 1 638 4000 Monte Carlo steps), and $L = 32$ (50 samples and 16 384 000 Monte Carlo steps).

We have found that the data (in the range of the lattice sizes we are able to simulate at this low temperature) are well described by power laws: the magnetization scales to zero as $L^{-0.25}$ and R_ξ as $L^{-0.15}$ (see Fig. 13). Notice that in a noncritical phase, with the thermodynamic correlation length greater than L, the behavior of this cumulant should be proportional to L^{-1}: hence, we are still simulating in the range of lattice sizes smaller than the asymptotic value of the correlation length.

Therefore, from this analysis, the behavior of the isotropic disorder at very low temperatures can be described by a phase with zero magnetization and finite correlation length in the magnetic channel. This result supports pretty well the behavior of the R_ξ cumulant and the magnetization around and below the second phase transition at β_c^2 described in Sec. IV B.

APPENDIX E: THE TWO-DIMENSIONAL $O(2)$ MODEL

In order to test the QLRO scenario for the IRAM, we have simulated the two-dimensional $O(2)$ model.

The most accurate analysis of this model has been performed in Ref. [106] reporting $\beta_c = 1.1199(1)$, $R_\xi = 0.7506912$, and $U_4 = 0.660603(12)$.

We have analyzed this model by studying the R_ξ and U_4 curves (see Fig. 14) using the fixed coupling method and neglecting scaling corrections. We report the results in Tables XI and XII. One can see from Fig. 14 that the correlation length data suffer from larger corrections to scaling than the Binder cumulant ones. Notice that the U_4 analysis provided with a value of the η exponent compatible with the analytical one ($\eta = 1/4$). Moreover, the ν exponents take very large values, eventually diverging in the thermodynamic limit, showing the fact that different curves of R_ξ and U_4 are merging in the low-temperature phase, which presents QLRO behavior.

TABLE XIV. Quotient method results for pure $O(3)$ model from the crossing points of U_4 for lattice sizes L_1 and L_2. The numbers between round brackets are the statistical error of the fit and the number inside the square ones are systematic errors originating from the uncertainty in the ω exponent used in the fit.

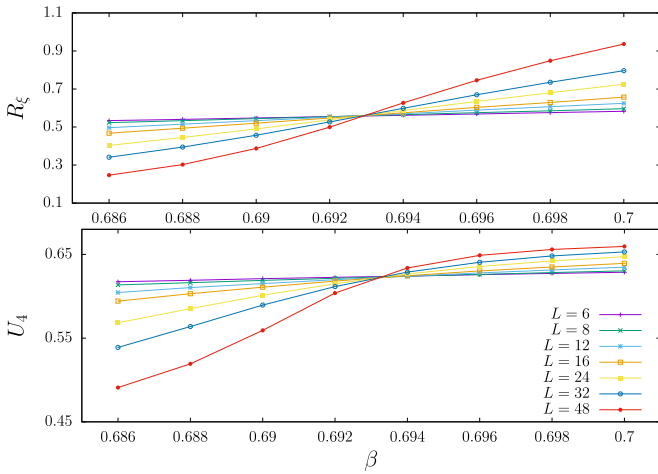| L_1/L_2	β_{cross}	U_4	ν_ξ	ν_{U_4}	η	Q_{U_4}
6/12	0.6942(1)	0.6243(2)	0.731(8)	0.728(3)	$-0.015(3)$	1.0168(7)
8/16	0.69368(5)	0.6236(1)	0.720(6)	0.718(2)	$-0.003(2)$	1.0130(6)
12/24	0.69320(3)	0.6223(2)	0.721(8)	0.716(3)	0.017(2)	1.0083(8)
16/32	0.69309(2)	0.6217(1)	0.720(8)	0.714(4)	0.021(2)	1.0064(8)
24/48	0.69305(2)	0.6214(1)	0.72(1)	0.716(6)	0.025(3)	1.005(1)
∞	0.69300(3)	0.6202(2)[2]	0.707(3)[1]	0.72(1)[1]	0.042(3)[3]	$\omega = 0.98(9)$

FIG. 17. R_ξ (top) and U_4 (bottom) cumulants against inverse temperature for the three-dimensional $O(3)$ pure model for several lattice sizes.

APPENDIX F: THE MAGNETIZATION AND R_ξ IN THE THREE-DIMENSIONAL EDWARDS-ANDERSON MODEL

To illustrate the behavior of some magnetic observables in a model with a spin-glass low-temperature phase, we have simulated two small lattices of the three-dimensional Edwards-Anderson model with binary coupling, which is a classic spin glass with zero magnetization. See Ref. [96] for additional details of the model (including Hamiltonian and observables).

In particular, we have simulated 1600 samples of $L = 6$ and 8 using the Metropolis and the Parallel Tempering

algorithms with 20 temperatures (204 800 Monte Carlo steps per temperature) around the infinite volume critical inverse temperature: $\beta_c = 0.908(2)$ [96].

Figure 15 shows the lack of criticality of this magnetization channel: R_ξ and U_4 are already compatible with zero, as should be.

However, the overlap channel clearly shows the PM-SG phase transition; see Fig. 16. In this figure, the curves for the cumulant R_{ξ_q} cross for the two different lattice sizes.

APPENDIX G: THE THREE-DIMENSIONAL $O(3)$ MODEL

In this Appendix we present our results on the three-dimensional $O(3)$ model using the quotient method with the same methodology as applied throughout the paper for the RAM.

We have run for this model $L = 6$, 12, 16, 24, 32, and 48 lattices, using parallel tempering with eight temperatures in the fixed range [0.686,0.700].

In Tables XIII and XIV we show the results of the quotient method for the crossing points of R_ξ and the Binder cumulant, respectively (see also Fig. 17). First, we have computed ω by fitting the last column to Eq. (B6). Once we have got this value, we perform all the fits of the rest of the columns using this ω value but for the inverse critical temperature (in this case, the correction is $1/\nu + \omega$, and we have left completely free this exponent in the fit). In the last row of these tables we have reported our extrapolations to infinite volume. The agreement, despite the small lattice sizes simulated, with the values reported in Table VII, is pretty good. In addition, the inverse critical temperature is fully compatible with the one reported in Ref. [107] [$\beta_c = 0.69300(1)$].

[1] Q. Luo, D. Q. Zhao, M. X. Pan, and W. H. Wang, Appl. Phys. Lett. **92**, 011923 (2008); Q. Luo and W. H. Wang, J. Non-Cryst. Solids **355**, 759 (2009); Q. Luo, B. Schwartz, N. Mattern, and J. Eckert, J. Appl. Phys. **109**, 113904 (2011).

[2] J. Hertz, Phys. Scr. T **10**, 1 (1985).

[3] Y. Holovatch, V. Blavats'ka, M. Dudka, C. von Ferber, R. Folk, and T. Yavors'kii, Int. J. Mod. Phys. B **16**, 4027 (2002).

[4] R. Harris, M. Plischke, and M. J. Zuckermann, Phys. Rev. Lett. **31**, 160 (1973).

[5] R. W. Cochrane, R. Harris, and M. J. Zuckermann, Phys. Rep. **48**, 1 (1978).

[6] D. J. Sellmyer and M. J. O'Shea, in *Recent Progress in Random Magnets*, edited by D. H. Ryan (World Scientific, Singapore, 1992), p. 71.

[7] Y. Goldschmidt, in *Recent Progress in Random Magnets*, edited by D. H. Ryan (World Scientific, Singapore, 1992), p. 151.

[8] M. Dudka, Y. Holovatch, and R. Folk, J. Magn. Magn. Mater. **294**, 305 (2005)

[9] J. M. D. Coey, J. Appl. Phys. **49**, 1646 (1978).

[10] For review, see E. M. Chudnovsky, in *The Magnetism of Amorphous Metals and Alloys*, edited by J. A. Fernandez-Baca and W.-Y. Ching (World Scientific, Singapore, 1992), p. 143.

[11] V. L. Berezinsky, Zh. Eksp. Teor. Fiz. **61**, 1144 (1972) [Sov. Phys. JETP **34**, 610 (1972)].

[12] J. M. Kosterlitz and D. J. Thouless, J. Phys. C **6**, 1181 (1983).

[13] U. Krey, Z. Physik B **26**, 355 (1977); J. Magn. Magn. Mater. **7**, 150 (1978); C. De Dominicis, Phys. Rev. B **18**, 4913 (1978); S.-K. Ma and J. Rudnick, Phys. Rev. Lett. **40**, 589 (1978); A. Khurana, Phys. Rev. B **25**, 452 (1982); S. Ciuchi and F. de Pasquale, Nucl. Phys. B **300**, 31 (1988); D. R. C. Dominguez and W. K. Theumann, J. Phys. A **28**, 63 (1995); M. Dudka, R. Folk, Y. Holovatch, and G. Moser, Condens. Matter Phys. **8**, 737 (2005); M. Dudka, R. Folk, Yu. Holovatch, and G. Moser, J. Phys. A **40**, 8247 (2007).

[14] A. A. Fedorenko and F. Kühnel, Phys. Rev. B **75**, 174206 (2007).

[15] A. A. Fedorenko, Phys. Rev. E **86**, 021131 (2012).

[16] E. Callen, Y. J. Liu, and J. R. Cullen, Phys. Rev. B **16**, 263 (1977); J. D. Patterson, G. R. Gruzalski, and D. J. Sellmyer, *ibid.* **18**, 1377 (1978).

[17] R. Harris and D. Zobin, J. Phys. F **7**, 337 (1977).

[18] B. Derrida and J. Vannimenus, J. Phys. C **13**, 3261 (1980).

[19] N. Sourlas, J. Phys. Lett. (France) **42**, 233 (1981).

[20] M. A. Continentino and S. Coutinho, J. Magn. Magn. Mater. **125**, 49 (1993).

[21] K. H. Fischer, Phys. Rev. B **36**, 6963 (1987).

[22] Y. Imry and S.-K. Ma, Phys. Rev. Lett. **35**, 1399 (1975).
[23] R. Alben, J. J. Becker, and M. C. Chi, J. Appl. Phys. **49**, 1653 (1978).
[24] D. J. Amit and V. Martín Mayor, *Field Theory, The Renormalization Group and Critical Phenomena* (World Scientific, Singapore, 2005).
[25] A. Aharony, Phys. Rev. B **12**, 1038 (1975).
[26] J.-H. Chen and T. C. Lubensky, Phys. Rev. B **16**, 2106 (1977).
[27] R. A. Pelcovits, E. Pytte, and J. Rudnick, Phys. Rev. Lett. **40**, 476 (1978).
[28] R. A. Pelcovits, E. Pytte, and J. Rudnick, Phys. Rev. Lett. **48**, 1297(E) (1982).
[29] R. A. Pelcovits, Phys. Rev. B **19**, 465 (1979).
[30] V. J. Emery, Phys. Rev. B **11**, 239 (1975).
[31] M. Dudka, R. Folk, and Y. Holovatch, Condens. Matter Phys. **4**, 77 (2001).
[32] M. Dudka, Yu. Holovatch, and R. Folk, in *Fluctuating Paths and Fields*, edited by W. Janke, A. Pelster, H.-J. Schmidt, and M. Bachmann (World Scientific, Singapore, 2001), p. 457.
[33] P. Calabrese, A. Pelissetto, and E. Vicari, Phys. Rev. E **70**, 036104 (2004).
[34] E. F. Shender, J. Phys. C **13**, L339 (1980).
[35] R. Fisch and A. B. Harris, J. Appl. Phys. **67**, 5778 (1990); Phys. Rev. B **41**, 11305 (1990).
[36] A. B. Harris, R. G. Caflisch, and J. R. Banavar, Phys. Rev. B **35**, 4929 (1987).
[37] Y. Y. Goldschmidt, Nucl. Phys. B **225**, 123 (1983).
[38] A. Khurana, A. Jagannathan, and M. J. Kosterlitz, Nucl. Phys. B **240**, 1 (1984).
[39] Y. Y. Goldschmidt, Phys. Rev. B **30**, 1632 (1984).
[40] A. Jagannathan, B. Schaub, and M. J. Kosterlitz, Nucl. Phys. B **265**, 324 (1986).
[41] D. Boyanovsky, Nucl. Phys. B **225**, 523 (1983).
[42] D. S. Fisher, Physica A **177**, 84 (1991).
[43] A. M. Khorunzhy, B. A. Khorunzhenko, L. A. Pastur, and M. V. Shcherbina, in *Phase Transitions and Critical Phenomena*, Vol. 15, edited by C. Domb and J. L. Lebowitz (Academic Press, London, 1992), p. 74.
[44] A. Aharony and E. Pytte, Phys. Rev. Lett. **45**, 1583 (1980).
[45] A. Aharony and E. Pytte, Phys. Rev. B **27**, 5872 (1983).
[46] J. Villian and J. F. Fernandez, Z. Phys. B **54**, 139 (1984).
[47] V. S. Dotsenko and M. V. Fiegelman, J. Phys. C **16**, L803 (1983).
[48] D. E. Feldman, JETP Lett. **70**, 135 (1999); Phys. Rev. B **61**, 382 (2000); Int. J. Mod. Phys. B **15**, 2945 (2001).
[49] D. S. Fisher, Phys. Rev. B **31**, 7233 (1985).
[50] M. Tissier and G. Tarjus, Phys. Rev. B **74**, 214419 (2006)
[51] P. Le Doussal and K. J. Wiese, Phys. Rev. Lett. **96**, 197202 (2006)
[52] Y. Sakamoto, H. Mukaida, and C. Itoi, Phys. Rev. B **72**, 144405 (2005); **74**, 064402 (2006); Y. Sakamoto, H. Mukaida, and C. Itoi, J. Phys.: Condens. Matter **19**, 145219 (2007).
[53] K. Ideura, Prog. Theor. Phys. **119**, 9 (2008); **121**, 897 (2009).
[54] D. Mouhanna and G. Tarjus, Phys. Rev. B **94**, 214205 (2016).
[55] D. Mukamel and G. Grinstein, Phys. Rev. B **25**, 381 (1982).
[56] A. L. Korzhenevskii and A. A. Luzhkov, Sov. Phys. JETP **67**, 1229 (1988).
[57] M. Dudka, R. Folk, and Y. Holovatch, Condens. Matter Phys. **4**, 459 (2001).

[58] V. Dubs, V. Prudnikov, and P. Prudnikov, Theor. Math. Phys. **190**, 359 (2017).
[59] D. Shapoval, M. Dudka, A. A. Fedorenko, and Y. Holovatch, Phys. Rev. B **101**, 064402 (2020).
[60] K. H. Fischer and A. Zippelius, J. Phys. C **18**, L1139 (1985).
[61] K. H. Fischer and A. Zippelius, Prog. Theor. Phys. Suppl. **87**, 165 (1986).
[62] D. R. C. Dominguez and W. K. Theumann, Phys. Rev. B **48**, 6234 (1993).
[63] M. C. Chi and R. Alben, J. Appl. Phys. **48**, 2987 (1977).
[64] R. Harris and S. H. Sung, J. Phys. F **8**, L299 (1978).
[65] M. C. Chi and T. Egami, J. Appl. Phys. **50**, 1651 (1979).
[66] R. Harris, J. Phys. F **10**, 2545 (1980).
[67] C. Jayaprakash and S. Kirkpatrick, Phys. Rev. B **21**, 4072 (1980).
[68] A. Chakrabarti, Phys. Rev. B **36**, 5747 (1987).
[69] R. Fisch, Phys. Rev. B **39**, 873 (1989).
[70] F. Parisen Toldin, A. Pelissetto, and E. Vicari, J. Stat. Mech. (2006) P06002.
[71] F. Liers, J. Lukic, E. Marinari, A. Pelissetto, and E. Vicari, Phys. Rev. B **76**, 174423 (2007).
[72] R. Fisch, Phys. Rev. Lett. **66**, 2041 (1991).
[73] R. Fisch, Phys. Rev. B **42**, 540 (1990).
[74] P. Reed, J. Phys. A: Math. Gen. **24**, L117 (1991).
[75] U. K. Rößler, Phys. Rev. B **59**, 13577 (1999).
[76] M. Itakura, Phys. Rev. B **68**, 100405(R) (2003).
[77] R. Fisch, Phys. Rev. B **79**, 214429 (2009).
[78] R. Fisch, Phys. Rev. B **48**, 15764 (1993).
[79] R. Fisch, Phys. Rev. B **58**, 5684 (1998).
[80] R. Fisch, Phys. Rev. B **51**, 11507 (1995).
[81] H. M. Nguyen and P.-Y. Hsiao, J. Appl. Phys. **105**, 07E125 (2009).
[82] A. I. Larkin, Zh. Eksp. Teor. Fiz. **58**, 1466 (1970).
[83] A. A. Berzin, A. I. Morosov, and A. S. Sigov, Phys. Solid State **58**, 2018 (2016).
[84] A. A. Berzin, A. I. Morosov, and A. S. Sigov, Phys. Solid State **59**, 2448 (2017); J. Magn. Magn. Mater. **459**, 256 (2018).
[85] K. Hukushima and K. Nemoto, J. Phys. Soc. Jpn. **65**, 1604 (1996).
[86] E. Marinari, in *Advances in Computer Simulation*, edited by J. Kerstész and I. Kondor (Springer, Verlag, Berlin, Heidelberg, 1998), pp. 50–81.
[87] R. Harman and V. Lacko, J. Multivariate Anal. **101**, 2297 (2010).
[88] F. Cooper, B. Freedman, and D. Preston, Nucl. Phys. B **210**, 210 (1982).
[89] H. G. Ballesteros, L. A. Fernandez, V. Martin-Mayor, A. Munoz-Sudupe, G. Parisi, and J. J. Ruiz-Lorenzo, Nucl. Phys. B **512**, 681 (1998).
[90] S. Wiseman and E. Domany, Phys. Rev. E **52**, 3469 (1995); A. Aharony and A. B. Harris, Phys. Rev. Lett. **77**, 3700 (1996).
[91] I. Campos, M. Cotallo-Aban, V. Martin-Mayor, S. Perez-Gaviro, and A. Tarancon, Phys. Rev. Lett. **97**, 217204 (2006).
[92] O. V. Billoni, S. A. Cannas, and F. A. Tamarit, Phys. Rev. B **72**, 104407 (2005).
[93] H. G. Ballesteros, L. A. Fernandez, V. Martin-Mayor, A. Munoz-Sudupe, G. Parisi, and J. J. Ruiz-Lorenzo, Phys. Rev. B **58**, 2740 (1998).

[94] J. A. Mydosh, *Spin Glasses: An Experimental Introduction* (Taylor and Francis, London, 1993).

[95] L. A. Fernandez, V. Martin-Mayor, S. Perez-Gaviro, A. Tarancon, and A. P. Young, Phys. Rev. B **80**, 024422 (2009).

[96] M. Baity-Jesi, R. A. Banos, A. Cruz, L. A. Fernandez, J. M. Gil-Narvion, A. Gordillo-Guerrero, D. Iniguez, A. Maiorano, F. Mantovani, E. Marinari *et al.*, Phys. Rev. B **88**, 224416 (2013).

[97] M. Campostrini, A. Pelissetto, P. Rossi, and E. Vicari, Phys. Rev. E **65**, 066127 (2002).

[98] M. Hasenbusch and E. Vicari, Phys. Rev. B **84**, 125136 (2011).

[99] M. Hasenbusch, J. Phys. A: Math. Gen. **34**, 8221 (2001).

[100] A. M. Ferrenberg, J. Xu, and D. P. Landau, Phys. Rev. E **97**, 043301 (2018).

[101] D. Simmons-Duffin, J. High Energ. Phys. 03 (2017) 086.

[102] A. Pelissetto and E. Vicari, Phys. Rep. **368**, 549 (2002)

[103] R. Folk, Y. Holovatch, and T. Yavors'kii, Uspiekhi Fizichieskikh Nauk **173**, 175 (2003) [Physics-Uspiekhi **46**, 169 (2003)].

[104] M. V. Kompaniets, A. Kudlis, and A. I. Sokolov, Phys. Rev. E **103**, 022134 (2021).

[105] D. A. Garanin and E. M. Chudnovsky, J. Phys.: Condens. Matter **34**, 285801 (2022).

[106] M. Hasenbusch, J. Phys. A **38**, 5869 (2005); J. Stat. Mech: Theor. Exp. (2008) P08003.

[107] H. G. Ballesteros, L. A. Fernandez, V. Martin-Mayor, and A. M. Sudupe, Phys. Lett. B **387**, 125 (1996).